Article

pubs.acs.org/Biomac

Supramolecular Organization in Self-Assembly of Chromatin and Cationic Lipid Bilayers is Controlled by Membrane Charge Density

Nikolay V. Berezhnoy,[†] Dan Lundberg,[‡,§,∥] Nikolay Korolev,[†] Chenning Lu,[†,⊥] Jiang Yan,[†] Maria Miguel,[‡] Björn Lindman,[‡,§] and Lars Nordenskiöld*[,†]

[†]School of Biological Sciences, Nanyang Technological University, 60 Nanyang Drive, Singapore 637551

[‡]Department of Chemistry, University of Coimbra, Rua Larga, 3004-535 Coimbra, Portugal

[§]Department of Physical Chemistry, Center for Chemistry and Chemical Engineering, Lund University, P.O. Box 124, 221 00 Lund, Sweden

Supporting Information

ABSTRACT: In this work we have investigated the structures of aggregates formed in model systems of dilute aqueous mixtures of "model chromatin" consisting of either recombinant nucleosome core particles (NCPs) or nucleosome arrays consisting of 12 NCPs connected with 30 bp linker DNA, and liposomes made from different mixtures of cationic and zwitterionic lipids, 1,2-dioleoyl-3-trimethylammonium-propane chloride salt (DOTAP) and 1,2-dioleoyl-*sn*-glycero-3-phosphocholine (DOPC). The aggregates formed were characterized using different optical microscopy methods and small-angle X-ray scattering (SAXS), and the results are discussed in terms of the competing intermolecular interactions among the components. For a majority of the samples, the presence of lamellar structures could be identified. In samples with high fractions of DOTAP in the liposomes, well-defined lamellar structures very similar to those formed by the corresponding lipid mixtures and DNA alone (i.e., without histone proteins) were observed; in these aggregates, the histones are expelled from the model chromatin. The findings suggest that, with liposomes containing large fractions of cationic lipid, the dominating driving force for aggregation is the increase in translational entropy from the release of counterions, whereas with lower fractions of the cationic lipid, the entropy of mixing of the lipids within the bilayers results in a decreased DNA–lipid attraction.

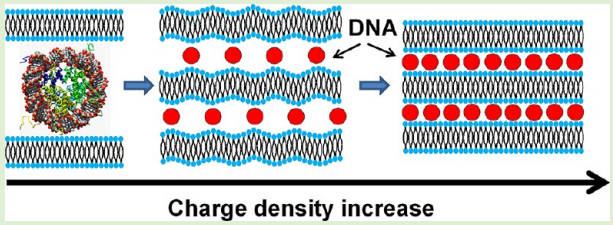

INTRODUCTION

The nucleus of the eukaryotic cell is a distinct compartment that is separated from the surrounding cytoplasm by the double-membrane nuclear envelope. In the nucleus, the DNA is combined with proteins into chromatin, a complex nucleoprotein with several levels of organization.[1,2] The fundamental structural unit of chromatin is the nucleosome core particle (NCP), which is composed of an octamer of histone proteins (two each of the core histones H2A, H2B, H3, and H4) around which 147 base pairs (bp) of DNA are coiled into a left-handed superhelix of about 1.7 turns.[3,4] The histones are rich in the basic amino acids lysine and arginine, and carry a net cationic charge that neutralizes half of the negative charge on the DNA, leaving the NCP with a net charge of about −150*e*. In chromatin, the NCPs are connected by 10–70 bp linker DNA in a beads-on-a-string arrangement, often referred to as the 10 nm fiber. The 10 nm fiber, in turn, is folded into a fiber with a diameter of approximately 30 nm and a debated structure.[5,6] The 30 nm fiber is further organized into higher-level arrangements.[7] Figure 1 illustrates the structure of the NCP and the nucleosome array and highlights the amphiphilic nature of the core histones that have a predominance of basic amino acid residues, but also exhibit extensive nonpolar hydrophobic regions.

The compaction of DNA into chromatin was for a long time mainly ascribed a "space-saving" function. This is indeed an important function: the 2 m of highly charged DNA containing the human genome, which in a random-coil conformation would occupy a sphere of ∼100 μm in diameter, is contained in a nucleus with a diameter of ∼10 μm. Although the underlying molecular mechanisms of DNA compaction into chromatin are not yet fully understood, it has become increasingly evident that a variation in the extent and type of higher order chromatin structure can be related to numerous DNA-related metabolic processes, including transcription, recombination, replication, and repair.[8−10] Thus, the structure of chromatin, which is heterogeneously distributed throughout the nucleus, is highly dynamic.

In addition to DNA and proteins, the eukaryotic nucleus contains a minor fraction of lipids, for instance, about 3% of the dry mass of rat liver nuclei; this lipid pool is constituted

Received: September 13, 2012
Revised: October 31, 2012
Published: November 6, 2012

 © 2012 American Chemical Society

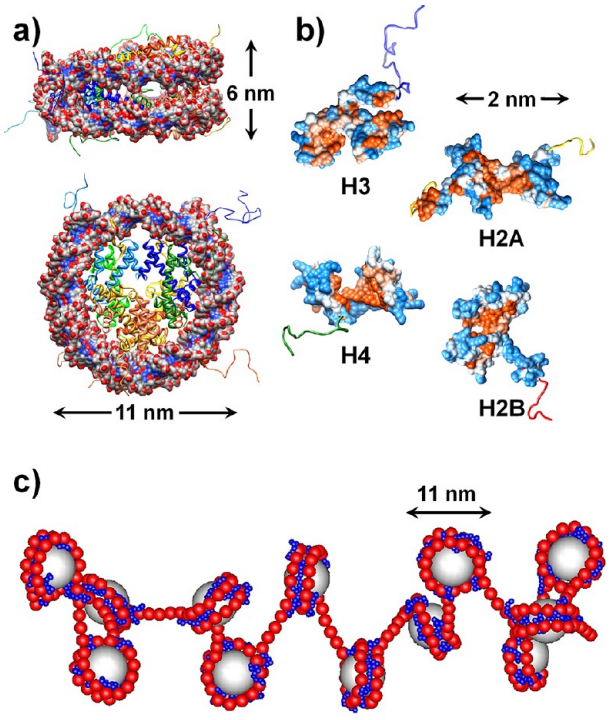

Figure 1. Illustrations of (a) an NCP, (b) the core histones, and (c) the nucleosome array. (a) Two projections of the NCP where DNA is shown as a surface with electrostatic potential (positive in red and negative in blue) and the histone octamer with schematic secondary structure (each of the eight histones is colored differently). Approximate dimensions of the NCP are indicated. The core histones shown in panel b illustrate the folded domains of each histone shown with the surface colored according to its electrostatic potential (positive in blue) and hydrophobicity (orange). To build structures a and b, the crystal structure of the NCP (1KX5) and the Chimera software were used. In panel c, the 12-177-601 nucleosome array is schematically shown with DNA (red) wrapped around the histone octamer core (light gray) with histone tails in blue.

predominantly of polar, thus amphiphilic, lipids.[11] A majority of the nuclear lipids reside in the nuclear envelope; thus these lipids have for a long time been ascribed mainly a structural role. Over later years it has been recognized, however, that the nuclear lipids perform additional functions. Particularly, the nonmembrane intranuclear lipids have been given increased attention. It is inherently difficult to ascertain accurate values of the quantity and composition of the intranuclear lipid pool. However, recent data suggest that, in certain instances, lipids can constitute as much as 10% of the intranuclear volume,[12] which motivates efforts to obtain an improved understanding of the interactions between chromatin and lipids.

Previously, the interactions between model chromatin and cationic liposomes were investigated by studying two different model systems for chromatin: one being the NCP, and the other being a nucleosome array of 12 NCPs connected with 30 bp linker DNA (Figure 1).[13] Phase-separating aggregates formed in dilute aqueous mixtures of either NCPs or nucleosome arrays with cationic liposomes were investigated using mainly small-angle X-ray scattering (SAXS), supplemented by cryo-transmission electron microscopy (cryo-TEM), and fluorescence microscopy. The structure of these aggregates was found to depend strongly on the fraction of cationic lipid in the liposomes. NCPs and arrays mixed with liposomes over a broad range of cationic lipid fractions formed a lamellar phase similar to that in control mixtures with corresponding DNA in the absence of protein, indicating the instability of DNA–histone complexes and dissociation of DNA from histones. Histone proteins were found to remain in the aggregates with lipids and DNA.[13] Only in a narrow range of very low fractions of cationic lipid were indications for structures of intact NCPs or arrays with liposomes identified. SAXS measurements revealed a characteristic distance of 160–170 nm, formed by NCPs sandwiched between two lipid bilayers, being prevalent in the aggregates.

The objective of the present work was to make an in depth investigation and arrive at a detailed understanding of the cationic liposome–chromatin systems. The main goal was to establish the supramolecular organization in the aggregates over a range of cationic liposome charge densities, and also to look into the location of histone proteins in the aggregates when NCPs/arrays are unstable, and a lamellar structure is formed. The NCPs and nucleosome arrays produced by recombinant technology have several advantages as model chromatin, being practically monodisperse and free from post-translational modifications. The cationic liposomes were made from mixtures of cationic and zwitterionic lipids, 1,2-dioleoyl-3-trimethylammonium-propane chloride salt (DOTAP) and 1,2-dioleoyl-sn-glycero-3-phosphocholine (DOPC), in molar ratios ranging from 3:97 to 100:0. In addition to the complexes formed with NCPs or arrays, reference samples with corresponding DNA were also investigated.

Systems containing cationic lipids and DNA have previously showed a behavior with great similarities to biologically more directly relevant systems of zwitterionic or anionic lipids and DNA in the presence of divalent ions.[14−16] As the cationic systems contain fewer components, they can constitute simple and well-defined model systems of relevance for understanding DNA-lipid interactions in general; the present work therefore serves as a model for approaching the general problem of understanding chromatin membrane interactions and self-organization of DNA, lipids and proteins. The understanding of the driving forces for such self-assembly may also aid in the design of biomolecular templates for nanofabrication of functional materials in delivery of both nucleic acids and drug molecules.[17] A large body of work on the behavior of mixtures of DNA and cationic amphiphiles is available, which comprises a valuable reference material to investigate complex systems as those herein investigated.[14,18−23] This work is motivated by the development and design of nonviral gene and other (e.g., siRNA) delivery approaches. Chromofection, gene delivery by protein transduction using chromatin, was suggested as an efficient means to deliver DNA to a variety of cells in a targeted fashion.[24] Improved DNA transfection efficiency was demonstrated using the histone H1 with cationic and anionic liposomes.[25,26] The present approach is therefore also motivated by the possibility to use core histones in combination with cationic lipids as a potential delivery vehicle.

MATERIALS AND METHODS

Preparation of the Histone Octamer from Recombinant Histone Proteins. The recombinant histones H2A, H2B, H3, and H4 from *Xenopus laevis* were refolded into histone octamers and used in the reconstitution of both NCPs and nucleosome arrays. The expression and purification of the histones, as well as the refolding of the histone octamers were performed as described in our previous work[27] based on procedures in previously published protocols.[28,29] Individual

dx.doi.org/10.1021/bm301436x | *Biomacromolecules* 2012, 13, 4146−4157

histones were expressed in the *Escherichia coli* BL21(DE3)-pLysS strain from Promega (Madison, USA), transfected with the pET-3a plasmid with histone coding sequences inserted into the *lac* operon. The cell lysate was sonicated to shear DNA. The histones segregated in inclusion bodies were purified by gel filtration on a Sephacryl S-200 column (ÄKTA FPLC, Uppsala, Sweden), in a SAUDE-1000 buffer composed of 7 M urea, 20 mM Na-acetate pH 5.2, 1 M NaCl, 5 mM 2-Mercaptoethanol and 1 mM EDTA, followed by ion exchange using a Resource S column (GE Healthcare, Uppsala, Sweden) in a gradient from 200 mM to 1 M NaCl.

The histone octamers were refolded from the pure H2A, H2B, H3, and H4 histones mixed at 1:1:1.2:1.2 molar ratios in an unfolding buffer containing 7 M Guanidine HCl, 10 mM Tris HCl pH 7.5 and 10 mM DTT. The octamer formation proceeded by the dialysis when guanidine was substituted by NaCl, and after dialysis the octamer was obtained in refolding buffer containing 2 M NaCl, 10 mM Tris-HCl pH 7.5, 10 mM 2-Mercaptoethanol and 1 mM EDTA. The octamer was purified from tetra/hexamers and unspecific aggregates by size exclusion fast protein liquid chromatography (FPLC) in the refolding buffer using a Superdex 10/300 GL column (GE Healthcare, Uppsala, Sweden). The concentration of the histone octamer was measured by UV absorbance spectroscopy using the relation that the optical density of 1 mg/mL octamer solution is 0.45 at λ = 276 nm (which is the maximum in absorbance due to tyrosine residues in histones being the only aromatic amino acid residues).

Preparation of DNA for NCPs and Nucleosome Arrays. The DNA molecules used in the reconstitution of the NCPs and the nucleosome arrays differ in origin and sequence. For generation of 147 bp DNA, used for the NCP preparation, the palindromic sequence originated from human α-satellite DNA was used.[3] To generate palindromic 147 bp DNA, a pUC19 plasmid construct containing 32 repeats of 84 bp DNA inserts was used. For generation of array DNA, the pWM530 plasmid construct containing a 2124 bp insert with 12 repeats of 177 bp (12_177_601) of Widom's 601 sequence[30] was used. Plasmids were amplified in the *Escherichia coli* HB101 strain and extracted by an alkaline lysis method.[31] RNA and protein contaminants were removed by RNase (Fermentas) treatment, phenol, chloroform-isoamyl alcohol extraction, and polyethelene glycol (PEG 6000) precipitation. Both plasmids were subsequently digested by EcoRV (New England BioLabs).

In the case of 147 bp DNA, the resulting 84 bp fragments were separated from the rest of the plasmid by PEG 6000, dephosphorylated by calf intestinal alkaline phosphatase (New England BioLabs), and digested by HinfI (New England BioLabs). The resulting 72 bp fragments with three-nucleotide overhang were purified by ion exchange chromatography using Mono Q column (GE Healthcare, Uppsala, Sweden) varying NaCl gradient from 0.3 to 1 M, and ligated using T4 ligase (New England BioLabs) to obtain 147 bp DNA.

In the case of array DNA, the 12_177_601 fragments were separated from the rest of the plasmid by PEG 6000 and purified by size exclusion chromatography using Sephacryl SF 1000 gel filtration column (GE Healthcare, Uppsala, Sweden).

Reconstitution of NCPs and Nucleosome Arrays. The reconstitution of NCPs and nucleosome arrays was done according to published methods.[29,32,33] The reconstitution of NCPs and arrays from histone octamers and 147 bp and 12_177_601 DNA, respectively, was performed by dialysis in a gradient from 1.3 to 0 M KCl in a buffer containing 20 mM Tris-HCl pH 7.5, 1 mM ethylene diamine tetraacetic acid (EDTA) and 1 mM dithiothreitol (DTT). The purity of the NCPs and arrays was assessed by electrophoretic mobility shift assay (EMSA) in 5% native polyacrylamide gel. The saturation of DNA by histone octamers in arrays was assessed by EMSA of arrays digested by ScaI (New England BioLabs).

Preparation of Liposomes. DOTAP and DOPC lipids were purchased from Avanti Polar Lipids, Inc. (Alabaster, AL, USA). Lipids dissolved in chloroform at 25 mg/mL were mixed in the desired molar concentrations, and dried under a stream of argon. The lipid film was hydrated by water to yield a solution of multilamellar vesicles at 25 mg/mL lipid concentration. The small unilamellar vesicles (SUVs) were obtained by either extrusion through 100 nm polycarbonate membrane using LiposoFast-Basic (Avestin, Inc., Canada) or by sonication until clarity, typically 15 min on ice using a tip sonicator Sonics vibra cell (Sonics & Materials Inc., USA). SUV solutions were centrifugated at 10 000*g* after sonication. All liposome solutions displayed monomodal distributions with polydispersity indices around 0.2 and mean diameters around 100 nm. The method of SUV preparation did not influence the lamellar distance as confirmed by SAXS.

Preparation of Lipid−Protein−DNA Aggregates. In the preparation of aggregates, DNA, NCP, or nucleosome array solutions were always mixed into the solution of liposomes. Mixtures were calculated with regard to the molar charge ratio (CR) of anions to cations. Single molecules of 147 bp DNA, array DNA, NCPs, nucleosome arrays, DOTAP, and DOPC have the total charge of −294*e*, −4248*e*, −148*e*, −2496*e*, +1*e*, and 0*e*, respectively. The preparation of samples for SAXS and microscopy is described in the corresponding sections below.

Microscopy. Fluorophore labeling of lipids, histones, and DNA was done in the same way for wide-field fluorescence and laser scanning confocal microscopy as described previously.[13] All fluorophores were purchased from Invitrogen (Carlsbad, CA, USA). Histone proteins were labeled with BODIPY FL STP ester sodium salt, following the manufacturer's protocol. The NCPs or the arrays were mixed with reactive dye in 10 mM HEPES buffer pH 7.5 and subsequently purified from free dye by either dialysis or centrifugation in Amicon tubes (Millipore, Billerica, MA, USA). DNA was stained by 4′,6-diamidino-2-phenylindole (DAPI) dihydrochloride that was added onto the glass slide. Liposomes were labeled by 0.2% molar Texas Red DHPE added to lipid mixtures dissolved in chloroform.

For wide-field fluorescence microscopy, solutions of NCPs were mixed with liposomes at a certain CR in order to obtain dispersed aggregates, in the range of the final total lipid concentration of 0.2−2 mg/mL.

Samples for laser scanning confocal microscopy and polarization microscopy were prepared in a different way from those for fluorescence microscopy. The resulting mixture of a 50 μg solution of arrays or DNA with liposomes was centrifuged, and the precipitate was transferred onto a glass slide for imaging. Whereas samples for fluorescence microscopy show the appearance of aggregates in solution, confocal and polarized images show precipitated aggregates, similar to the observations for samples for SAXS.

The fluorescence and polarized light microscopy samples were imaged by an Eclipse 90i microscope (Nikon Corporation, Tokyo, Japan) using Nikon Plan Fluor 100×/1.30 Oil, and Plan Fluor 20×/0.5 objectives, respectively. Images were captured by MicroPublisher 5.0 RTV camera (Qimaging,

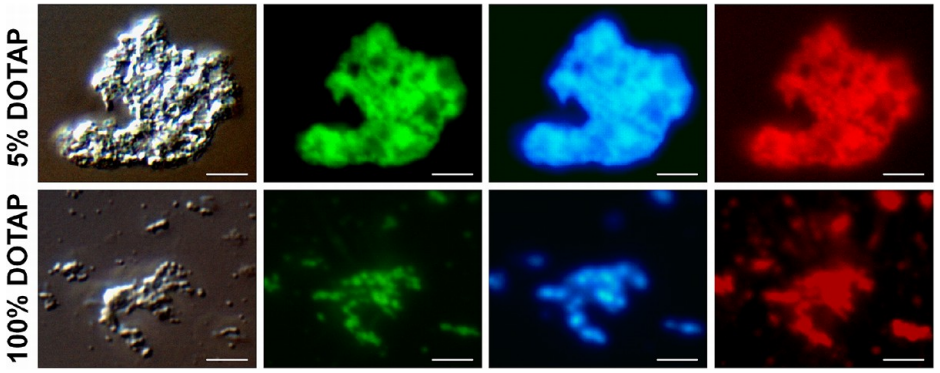

Figure 2. DIC and fluorescent microscopy images showing colocalization of DNA, lipids and proteins in aggregates of NCPs with 5% and 100% DOTAP, and with CR = 0.5 and lipid concentrations of 2 mg/mL and 0.2 mg/mL, respectively. Histones were labeled by BODIPY (green), DNA by DAPI (blue), and liposomes by Texas Red conjugated to the head of DHPE (red). The scale bar is 5 μm.

Surrey, BC, Canada) and analyzed by the Image-Pro Express software version 5.0.1.26 (Media Cybernetics, Inc., Rockville, MD).

Confocal microscopy images were obtained by a Zeiss LSM 710 microscope using a Zeiss Plan-Apochromat 63×/1.40 oil objective. Images were analyzed by ZEN (Carl Zeiss Micro-Imaging GmbH, Germany) and Huygens Essential (Scientific Volume Imaging B. V., Hilversum, The Netherlands) softwares.

Small-Angle X-ray Scattering. SAXS samples were prepared from equal volumes of solutions of liposomes and solutions of NCPs/arrays/DNA. An initial mixing was done in a plastic tube. After thorough mixing, the solutions with aggregates were transferred to quartz capillaries with 1.5−2 mm diameter (Charles Supper Company, MA, USA). Capillaries were sealed by wax and were centrifuged at around 1000*g* to precipitate the aggregates. The lipid concentrations in the SAXS samples were in the 1−20 mg/mL range. The lipid concentration influenced only the amount of the aggregates, but not the lamellar structure as confirmed by SAXS.

SAXS measurements were conducted at the BL23A SWAXS endstation at the National Synchrotron Radiation Research Center, Hsinchu, Taiwan. Samples were measured at ambient temperature (~25 °C). With a 14.0 keV beam (wavelength λ= 0.886 Å) and a sample-to-detector distance of 1.75 m, SAXS data were collected using an area detector (MarCCD165, Mar USA, Evanston, IL). The scattering wave vector $q = (4\pi \sin \theta)/\lambda$ (with 2θ the scattering angle) was calibrated using silver behenate. A typical data collection time was 100 s. SAXS profiles were circularly averaged from the isotropic 2-D patterns measured. All the SAXS data were corrected for sample transmission, background scattering, and detector noise, following a standard procedure described previously.[34] Although we have measured complexes equilibrated for a few days, no significant change in the diffraction spectra was detected after 6 months. The positions and full widths at half-maximum (fwhm) of diffraction peaks were obtained by fitting spectra to a Lorentzian or Gaussian functions using Peak Analyzer in the OriginPro 8 software (Northampton, MA, USA).[35] On one occasion, SAXS data was also collected at the X33 EMBL BioSAXS beamline located at DESY (Hamburg, Germany), and no discrepancy in data quality was found. In the presentation of numerical results obtained from the position and width of the diffraction peaks, in cases where the number of independent measurements n was more than one (2−5), an average value is shown with the standard deviation indicated by error bars.

RESULTS

Visual Observations. In mixtures of cationic liposomes with NCPs, nucleosome arrays, or the corresponding DNA molecules, phase separation was observed down to submillimolar concentrations of lipid. In a series of samples with a constant lipid concentration of 0.14 mM (~0.1 mg/mL), particles scattering light were detected in the 5−100% DOTAP and 0.25−2 CR ranges. The tendency for formation of a macroscopic precipitate was highest close to CR = 1, corresponding to equal concentrations of opposite charges.

For more concentrated samples (10−20 mg/mL with respect to total lipid), a clear dependence of the visual appearance of the precipitate on the fraction of cationic lipid in the liposomes was identified. NCPs or array aggregates with high charge density liposomes formed dense and white opaque precipitate, while soft, translucent, and "gel-like" precipitate was formed with low charge density liposomes. The precipitate with NCP and 100% DOTAP liposomes was estimated to be about 1.6 times denser than the precipitate with 5% DOTAP (Figure S1, Supporting Information), assuming that all the solutes in the mixture are found in the precipitate. In comparison, precipitated DNA−lipid aggregates appear dense and white opaque at all charge densities. The presence of histone proteins, therefore, is essential for the soft and gel-like appearance of low charge density liposome−DNA aggregates.

Comparison on the Micrometer Scale by Optical Microscopy. A number of optical microscopy techniques was used to further investigate the differences between the aggregates formed with liposomes of high and low DOTAP fractions.

Differential interference contrast (DIC) microscopy images, exemplified in Figure 2, showed that the aggregates prepared with liposomes of 5% DOTAP appeared as homogeneous lumps with typical dimensions of tens of micrometers, whereas those formed with liposomes of 100% DOTAP consisted of dispersed or loosely attached smaller and denser granules.

In order to estimate the extent of colocalization of DNA, proteins, and lipids in the aggregates formed, samples where each component was labeled with a different fluorescent probe were studied by fluorescence microscopy. The resulting micrographs, exemplified in Figure 2 for samples with 5% and 100% DOTAP, showed that lipid, DNA, and histones were colocalized with a diffraction-limited resolution around 0.2 μm. It was noted that the average size of the observed aggregates in

solution was larger in mixtures where the CR was close to unity than with excess of either of the components (data not shown).

Laser scanning confocal microscopy was used to investigate colocalization with twice as high resolution in the optical axis, in comparison with the wide field microscopy.[36] Figure 3 shows

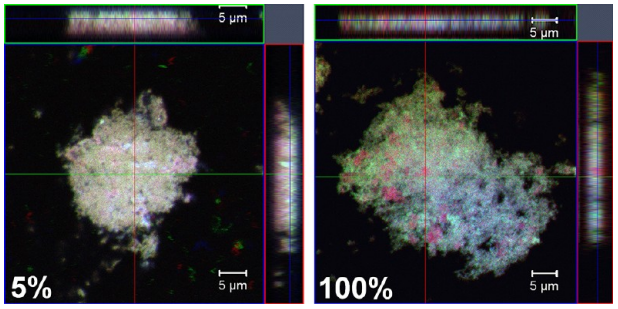

Figure 3. Confocal microscopy images of triple labeled aggregates of arrays and liposomes at 5% and 100% DOTAP, CR = 1. The images were obtained from the focal plane 1 μm thick found 3 μm inside the aggregates (top and right panels). The homogeneous color distribution at 5% DOTAP indicates a complete colocalization of DNA, histone proteins, and lipid bilayers in both the focal plane and the optical axis. The aggregates at 100% DOTAP, however, display regions of green and red aggregates, indicating dissociation of histone proteins from DNA and an expulsion from the lamellar phase.

the superposition of the three fluorescence signals for aggregates collected from samples prepared with 5% or 100% DOTAP. A comparison between these two images shows that there is a more homogeneous distribution of DNA, histones, and lipid in the aggregate with 5% DOTAP than with 100% DOTAP. In the latter case, the appearance of red and green patches indicates a partial segregation of lipids and histones.

Anisotropic supramolecular aggregates, such as liquid crystalline lamellar lipid phases, are optically birefringent and show distinct optical textures when placed between crossed polarizers and viewed in an optical microscope.[14,37] When investigated in a microscope, aggregates formed with liposomes with high fractions of DOTAP and NCPs, arrays, or the corresponding DNA molecules, are clearly birefringent and show patterns characteristic of a lamellar phase. Birefringence was found to be related to the fraction of cationic lipid in the liposomes: with a decrease in the percentage of DOTAP, a gradual decrease of the birefringence was observed with a virtual absence of birefringence at 5% DOTAP in mixtures with NCPs (Figure 4). The appearance under crossed polarizers of mixtures with nucleosome arrays and corresponding DNA molecules is shown in Figure S2, Supporting Information.

Characterization on Nanometer Scale by SAXS. Synchrotron SAXS was used to obtain information on the nanoscale supramolecular organization of the aggregates formed in the mixtures of liposomes with either NCPs, arrays, or DNA. Influence of two variables in the composition of aggregates was investigated, i.e., the mole percentage of cationic lipid in the liposomes, which ranged from 3 to 100% DOTAP, and the CR of the mixture, which covered a range of 0.5−2. Mixtures with CR = 1 have equimolar numbers of anionic and cationic charges, and hence a complete neutralization is expected.

Figure 5 compares SAXS spectra from samples with NCPs and 147 bp DNA (Figure 5a,b), and nucleosome arrays and

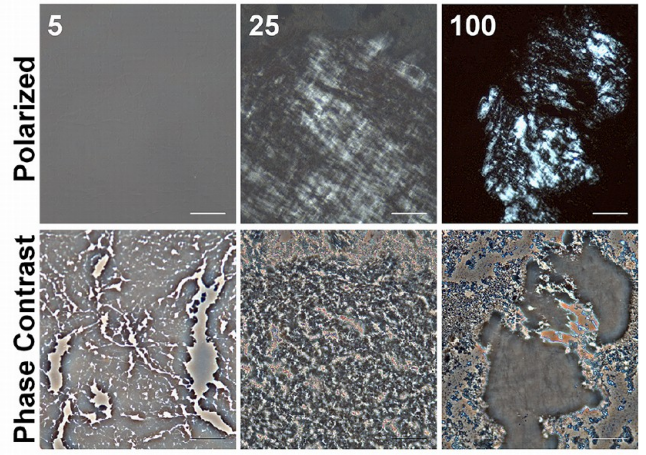

Figure 4. Polarized light and phase contrast micrographs of aggregates of NCPs and liposomes with 5%, 25% and 100% DOTAP at CR =1. The birefringence in polarized light, characteristic of lamellar phase, is observed to gradually increase with an increase in the fraction of DOTAP. Whereas the birefringence is absent at 5% DOTAP, and has the strongest intensity at 100% DOTAP, the intensity is intermediate at 25% DOTAP. The scale bar is 50 μm.

array DNA (Figure 5c,d) at CR = 1 at different DOTAP percentages.

The scattering profiles from the samples of the four series show significant similarities with respect to the dependence on the liposome composition. All samples show Bragg peaks $(0,0,q_n) = nq_0 = n2\pi/d_L$ (with harmonic order n = 1, 2, 3...) consistent with a DNA-lamellar phase,[14] where q is the scattering vector, and d_L is the lamellar repeat distance. In our systems, the lamellar peaks q_{001} and q_{002} appear around q = 0.1 and 0.2 Å^{-1}, respectively. The value of the lamellar distance, d_L, i.e., the interlayer spacing of the lamellar phase, that is, the sum of the lipid bilayer thickness and that of the water layer with DNA molecules, is obtained from the position of the first lamellar peak, q_{001}, using the following equation:

$$d_L = \frac{2\pi}{q_{001}} \quad (1)$$

Figure 6 compares the values of d_L, calculated from the profiles in Figure 5 using eq 1, as a function of liposome composition for the sample series with NCPs, nucleosome arrays, and corresponding DNAs at CR = 1. A similarity of monotonic decrease in d_L for all samples above 50% DOTAP, and an increase in d_L for NCPs and arrays compared to the corresponding samples with only DNA below 50% DOTAP was observed for all aggregates in a range of CR from 0.5 to 2 (see Figure S3 illustrating data for CR = 0.5 and 2). The variation in d_L as a function of CR in the range 0.5−2 was found to be insignificant (see Figure S4 illustrating the variation of d_L at different CR values for the NCPs); therefore, the presentation and discussion will focus on data at CR = 1. No significant differences in spacing between the two sizes of DNA (147 bp or 2124 bp) were observed at all lipid charge densities.

Lamellar peaks from the spectra in Figure 5 appear as circular Scherrer rings when the two-dimensional scattering is considered, which indicates the existence of isotropically oriented lamellar domains in the precipitate. Such submicrometer lamellar domains have been directly observed previously using cryo-TEM.[13,38] The finite domain size causes

dx.doi.org/10.1021/bm301436x | Biomacromolecules 2012, 13, 4146−4157

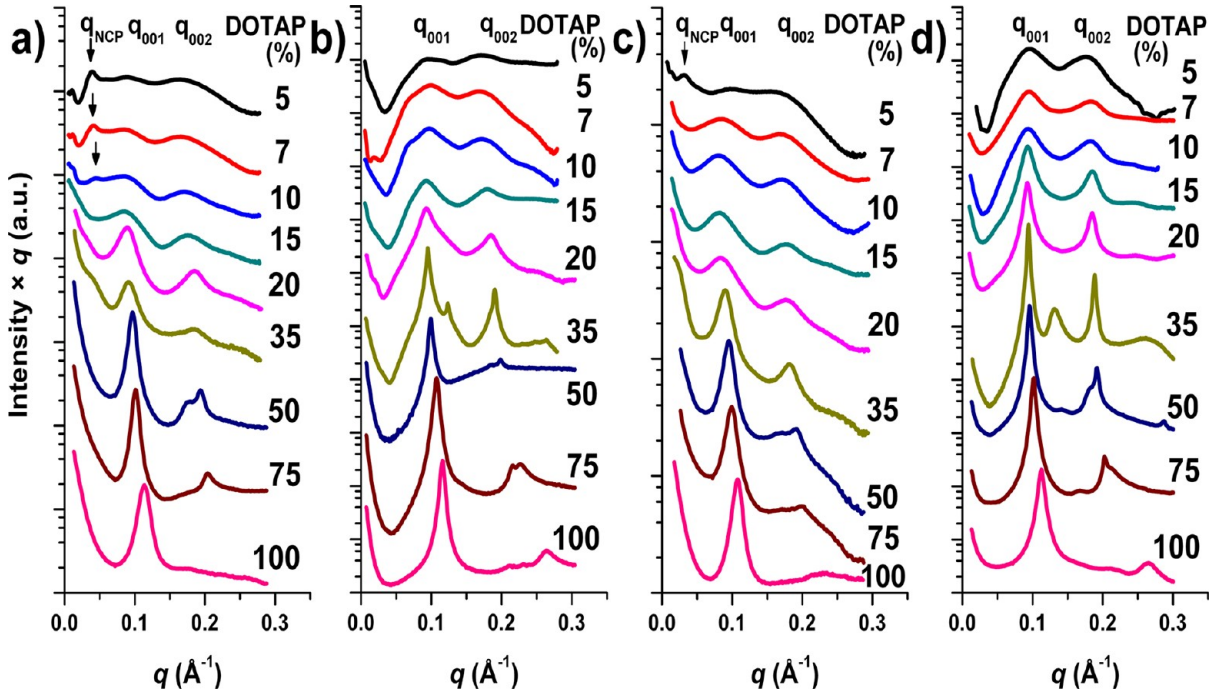

Figure 5. SAXS spectra of selected samples obtained from mixed solutions of liposomes of different percentages of DOTAP (indicated at the respective curves) and (a) NCPs, (b) 147 bp DNA, (c) nucleosome arrays, or (d) array DNA. In all cases, CR = 1. Spectra were shifted along the intensity axis for better visualization. Arrows indicate the q_{NCP} peaks found in samples with NCPs and arrays at low percentages of DOTAP; the positions of the first and second lamellar peaks are indicated as q_{001} and q_{002}, respectively.

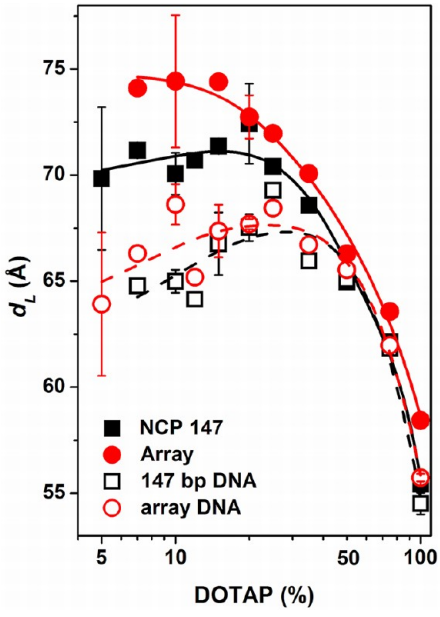

Figure 6. Comparison of the lamellar distance at CR = 1 in cationic liposome mixtures with NCPs, nucleosome arrays, and the corresponding DNA molecules. At a high percentage of DOTAP, all four mixtures display similar lamellar distances. At low percentages of DOTAP, both 147 bp DNA and array DNA produce similar values of d_L, while NCPs and nucleosome arrays display larger lamellar distances. Mixtures with arrays display larger lamellar distances than NCPs. Error bars represent the standard deviations. The lines are guides to the eye obtained from the data interpolation.

a symmetric broadening of the lamellar peaks, hence fitting of Lorentzian or Gaussian functions can be used to estimate the width of lamellar peaks.[35] The lower boundary of the effective domain size, s, of the lamellar phase can be estimated using a relation similar to eq 1, namely $s \approx 2\pi/\text{fwhm}$,[39] where fwhm is the full width at half-maximum of the first lamellar peak. The sizes of these domains were found to be on the order of submicrometers. The corresponding sizes of the lamellar domains are 60, 40, and 100 nm for the NCP, array, and both DNA systems, respectively. From the knowledge of the effective domain size s and the lamellar distance d_L for a particular fraction of DOTAP, the number of lamellar layers per domain (n_L) can be calculated using the relation $n_L = s/d_L$. Figure 7 shows that in precipitates with NCPs and arrays in comparison with the corresponding DNA molecules, increase in peak width and decrease in the number of lamellar layers per domain are observed. The number of layers per domain in aggregates with NCP and array decreases with the fraction of DOTAP and reaches minimum at 20% of DOTAP. Note how the estimated minimum of around two lamellar layers per effective domain approaches the theoretical limit of a single lamellar domain. We did not consider the contribution to the structure factor due to a variation of lamellar distances that can be caused by lipid bilayer undulations that may become significant at low charge densities.

For NCP samples prepared with 10% DOTAP and below, and for array samples with 5% DOTAP and below, peaks at q values of about 0.03−0.04 Å^{-1} were observed. Representative spectra with these typically rather sharp peaks are shown in Figure 8a. The intensity of these q_{NCP} peaks depended significantly on the CR for a constant lipid composition (as can be inferred comparing spectra from Figure 8 with those for the corresponding samples at CR = 1 from Figure 5). Although the sharpest peaks were observed for aggregates with NCPs at CR = 2, peaks at CR 1 are displayed in Figure 5, and Table 1 lists the positions and the corresponding characteristic distances (using eq 1) for all q_{NCP} peaks observed in aggregates

dx.doi.org/10.1021/bm301436x | Biomacromolecules 2012, 13, 4146−4157

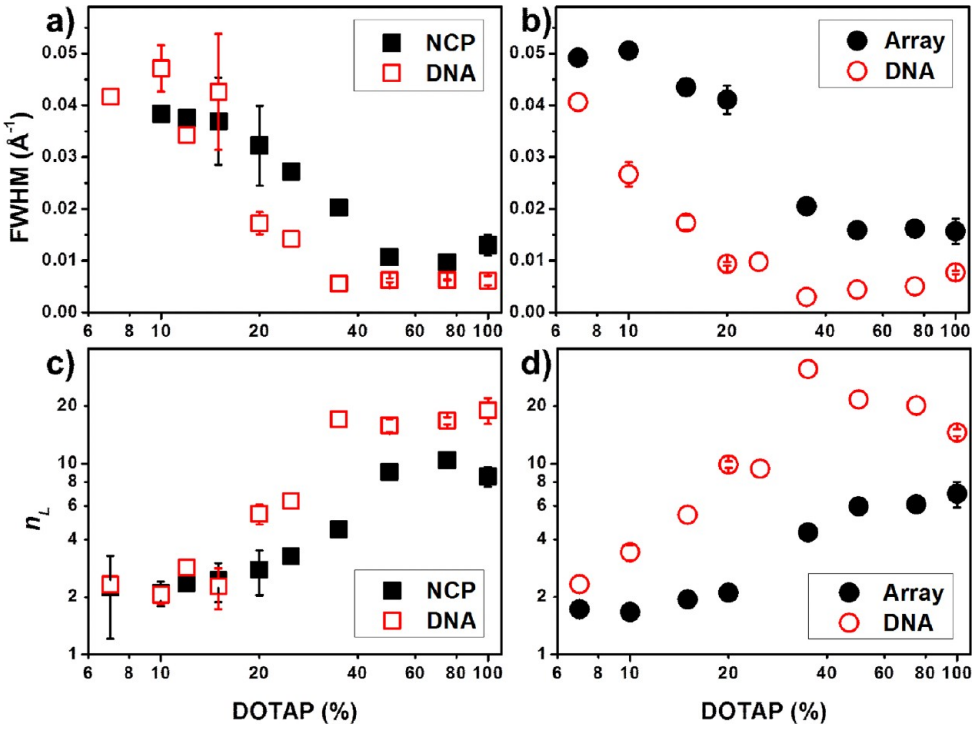

Figure 7. Lamellar phase characteristics as a function of liposome charge density, given as the percentage of DOTAP. The width of the first lamellar peak (a) and the number of layers (n_L) (c) are compared for NCPs and the corresponding 147 bp DNA. The same comparison between nucleosome arrays and the corresponding array DNA is presented in panels b and d, respectively. All complexes were prepared at CR = 1. The error bars represent the standard deviations.

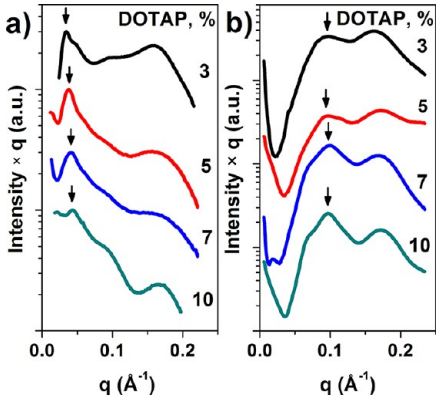

Figure 8. SAXS spectra from aggregates formed by liposomes with low percentages of DOTAP and NCPs compared with those of DNA without proteins. (a) Spectra from NCP–liposome aggregates at CR = 2; arrows indicate q_{NCP} peaks. (b) Spectra from 147 bp DNA–liposome mixtures at CR = 1; black arrows indicate lamellar peaks. Peaks identified by arrows that were observed in mixtures of NCPs with the low charge density liposomes are absent in control mixtures with DNA.

of liposomes and NCPs/arrays. It should be noted that even the sharpest peaks were still broad, thus the corresponding characteristic distances obtained from the peak positions should be regarded as estimates only; they are not as precise as in the case of the lamellar distances. Nevertheless, the obtained distances correspond well to a condition where intact NCPs are positioned between the two lipid bilayers. The scattering signals from such structures appear rather weak.

Importantly, as illustrated in Figure 8b, the low-q peak is absent in profiles from samples with DNA only. The shoulders appearing at a q of ~0.075 Å^{-1} in the profiles for samples with 7 or 10% DOTAP in Figure 8b can tentatively be attributed to the coexistence of DNA lamellar phase with a fraction of a more swollen, DNA-free lamellar phase. In previous reports on lamellar phases of DOTAP, DOPC, and DNA, such a phase segregation of DOPC has been noted.[40]

DISCUSSION

The experimental findings consistently show that there is a distinct variation in the character of the precipitates formed when NCPs as well as arrays are mixed with liposomes of different lipid compositions, i.e., with varying bilayer charge density. A systematic characterization of the aggregates in the whole composition range reveals three different types of aggregates, formed at high, intermediate, and low charge densities of lipid bilayer. The sharp reflections in the SAXS profiles and the distinct birefringence patterns in polarized light microscopy observed for samples with high bilayer charge density suggest that ordered lamellar structures are formed. From the SAXS data one can conclude that these lamellar structures show great similarities to those formed with the corresponding lipid mixtures with DNA alone (i.e., in the absence of histone proteins). When the bilayer charge density is intermediate, a decrease in size of lamellar domains is observed to accompany an increase in the repeat distance. The greater increase in lamellar distance, in comparison with corresponding lipid mixtures with DNA alone, indicates that histone proteins are included in the lamellar structure. At the low liposome charge densities, samples are significantly different on several points. For these compositions, the precipitates show a soft, swollen appearance, which suggests a significant retention of water in the structure. Furthermore, the reflections corresponding to the lamellar organization are broad and low in intensity

dx.doi.org/10.1021/bm301436x | *Biomacromolecules* 2012, 13, 4146–4157

Table 1. Positions of the q_{NCP} Peaks and the Corresponding Characteristic Distances for Samples of Varying Compositions[a]

	NCP 147						nucleosome arrays			
	0.5[b]		1		2		0.5		1	
DOTAP, %	peak, Å^{-1}	d, Å	peak, Å^{-1}	d, Å	peak, Å^{-1}	d, Å	peak, Å^{-1}	d, Å	peak, Å^{-1}	d, Å
3	[c]				0.033	190			0.031	201
5	0.037	168	0.037	172	0.038	166	0.035	178	0.031	202
7	0.031	203	0.039	161	0.04	157				
10			0.044	142	0.043	146				

[a]Selected samples have been measured more than once, and reproducibility was found to be better than 10%. [b]CR value of the mixture. [c]No low q-peaks have been observed.

(and for the lowest DOTAP contents practically absent) and the samples show only a weak birefringence pattern in polarized light microscopy. Importantly, samples with the lowest DOTAP fractions and NCPs or nucleosome arrays, but not samples with DNA only, show rather sharp peaks at q values in the range of ∼0.03−0.05 Å^{-1} in the SAXS profiles.

Because of the large number of components involved in the herein investigated systems, a discussion on the formation of possible structures based on the intermolecular interactions is rather challenging. Therefore, before discussing and interpreting the findings in any detail, the behavior of simpler aqueous mixtures of the involved or related components will first be considered. Mixtures of oppositely charged polyelectrolytes, or of a polyelectrolyte with aggregates of an oppositely charged amphiphile, show a strong propensity for association and formation of a phase concentrated in both species. The dominant driving force for this association is the gain in translational entropy from a release of the simple counterions to the surrounding solution.[41] Examples are the complexes formed by DNA and cationic lipids (or net-cationic lipid mixtures), which, due to their importance as vehicles in nonviral gene therapy, have been extensively investigated over the last few decades.[38,42,43] An increase in entropy caused by the release of simple counterions is also of major importance in the formation of the NCPs and chromatin from the highly negatively charged DNA polyion and the positively charged histone octamer, as it is well documented that the entropy gain from the counterion release is the major free energy contribution in DNA binding to cationic ligands[44−46] and to a wide variety of proteins.[47] A similar mechanism is considered in recent works with applications to chromatin.[48−50] The formation of the histone octamer itself, however, is driven mainly by hydrophobic interactions, and, because of the rather high net cationic charge of each of the histones, the octamer is stable in solution in the absence of DNA only at elevated ionic strengths, i.e., above 0.5 M of monovalent salt.[51,52] A major part of the hydrophobic surfaces is buried upon formation of the histone H2A/H2B dimer and the $(H3/H4)_2$ tetramer, an association that is preceding the stoichiometric complex formation of all four histones to form the complete octamer. If the NCPs dissociate, the hydrophobic domains of the histones can interact with other species or they may self-associate (see Figure 1). In this context, it deserves mention that although DNA carries hydrophobic domains as do histones, the amphiphilicity of single-stranded DNA is a crucial driving force in the formation of the familiar double helix[53] and hydrophobic interactions can be important in DNA−ligand interactions;[54] however, the extent of hydrophobic interactions between dsDNA and amphiphiles is very limited.[55] It can thus be regarded as a highly charged polyion that will interact with the lipid bilayers predominantly by electrostatic interactions.

Another effect to consider is that of a reduction of the charge density of the lipid bilayers as DOTAP is mixed with DOPC. When different amphiphiles (lipids, surfactants, etc.) are mixed in aqueous solution, there is typically a strong propensity for the formation of mixed aggregates, which can be attributed to an increase in the translational entropy of mixing. Only in cases where the involved hydrophobic parts are very different in character there will be a counteracting tendency for segregation. In the herein discussed lipid mixtures, where both DOTAP and DOPC carry oleoyl chains, there is no tendency of segregation caused by tail incompatibility. When an amphiphilic mixture contains both a nonionic (or zwitterionic) and an ionic component, an additional driving force for mixing is the increase in counterion entropy on mixing; a well-known consequence of this entropy increase is the decrease in the values of the critical micelle concentrations (CMCs) of mixtures of ionic and nonionic surfactants (as manifested by negative values of the so-called β parameter).[56]

When a lamellar structure is formed from DNA and lipid bilayers containing a low fraction of cationic lipid, the latter has to be locally concentrated in the vicinity of the DNA double helices to avoid a need for inclusion of mobile counterions in the precipitate. It has been found from NMR studies, as well as computer simulations, that aggregates of DNA and mixtures of cationic and uncharged (zwitterionic) amphiphiles indeed show a locally elevated concentration of the cationic component close to the DNA.[57−61] The lower the fraction of DOTAP in the lipid mixture, the higher the entropic penalty will be for the concentration of the cationic lipid close to the highly charged DNA, which, in turn, contributes to a larger free energy change for the formation of multilamellar bilayers with DNA sandwiched in between. At an intermediate lipid composition, a delicate balance may be expected between the gain in entropy from a uniform distribution of the cationic lipid and its counterions over the lipid bilayer, and the gain in entropy from the release of the counterions of the DNA as well as the lipid upon association of the two.

While thermodynamic arguments based on intermolecular interactions must be the basis for the discussion, it is important to remember that these arguments, strictly speaking, apply only to an equilibrium situation. Here we deal with metastable states in different respects. To give two examples: First, the liposomes do not represent an equilibrium state, but are metastable dispersions of a lamellar phase. Second, the associative phase separation initially typically leads to metastable colloidal particles rather than a separate macroscopic phase, which can take a very long time to equilibrate. Although we did not aim at systematic equilibration of the samples over extended time

periods, several samples had been studied after equilibration over 4 months. X-ray diffraction spectra remained essentially unchanged, and we did not observe any indications of novel structures arising on a longer scale.[62]

The structure of a complex between DNA and cationic lipids is largely controlled by the structures of the lipids used; these dictate the preferred curvature of the surface of the lipid aggregates. For the specific case of DOTAP:DOPC mixtures, it has previously been found that well-defined lamellar liquid crystalline structures, with the DNA double helices sandwiched between parallel lipid bilayers, are formed in a wide range of compositions.[14] The herein found decrease in the lamellar distance with an increase in the fraction of DOTAP from 30 to 100% (Figure 6) is consistent with the data presented in the literature.[35] The polar headgroup of DOPC has a larger volume than that of DOTAP, leading to 4−5 Å length difference. However, as the DOTAP is expected to be concentrated close to the DNA, it is not likely that the variation in lamellar distance is caused only by the difference in headgroup volume. With 100% DOTAP, the charge matching between DNA and the lipid bilayers is close to perfect.[40] As the charge density of the lipid bilayer is decreased, with an increasing fraction of DOPC, one can, as discussed above, expect an entropic penalty for the concentration of the cationic lipid in the vicinity of the DNA chains. It is likely that it is overall favorable to include a fraction of the counterions, and that an osmotic swelling of the water layer due to entrapped ions could contribute to the increase in d_L with decreasing DOTAP fraction in the lipid mixture.

Because of the high stiffness of double-stranded DNA, there is typically a high directional correlation between the DNA chains, i.e., they lie practically parallel between the lipid layers. This ordering of the DNA molecules often gives rise to a rather distinct correlation peak in SAXS profiles from cationic lipid−DNA complexes; such a correlation peak is clearly distinguishable at around a q value of 0.15 $Å^{-1}$ in the profiles corresponding to 35% DOTAP in Figure 5b,d. The DNA chains can be expected to be more ordered at higher charge density of the lipid film, and arranged in parallel practically side-by-side with very little intervening space as in the case of lipid bilayers of 100% DOTAP. The change in the position of the DNA−DNA correlation peak indicates an increased distance between parallel DNA rods upon decreasing liposome charge density;[14] results for the NCP or array systems display a behavior similar to the corresponding systems with DNA alone (see Supporting Information Figure S5).

Organization of Aggregates at the High Charge Densities. In agreement with previous findings,[11,14,40,63] and as discussed above, the lamellar structure of aggregates in samples prepared with liposomes containing a high fraction of DOTAP and NCPs or nucleosome arrays show major similarities to the structure of aggregates in the samples of the corresponding lipid mixtures and DNA in the absence of proteins. Almost identical lamellar distance values are observed to monotonically decrease for NCPs and DNA as well as for arrays and DNA in the 50−100% DOTAP range (Figure 6). Figure 7 shows that during the significant change in d_L, the number of lamellar layers per domain remains nearly constant. The average domain size is the only difference observed in the 50−100% DOTAP range between NCP or array systems and corresponding DNA systems. The SAXS data thus suggest that the presence of histones in this composition range affects the lamellar phase by decreasing the domain size nearly by a factor of 2, but has no significant influence on repeat distance of the lipid−DNA lamellar phase. From geometrical arguments one can deduce that the inclusion of protein in these lamellar structures must be restricted. As was mentioned above, the DNA−lipid charge matching is close to perfect with 100% DOTAP,[14,64] which means that there, at least in this composition, simply is not much space left in the structure. The histones must thus to a large extent be separated from the DNA. They have a lower charge density than that of the lipid aggregates and will associate less strongly with DNA.

The exclusion of the histones from the lamellar structure can be explained by the mixing of the NCPs/arrays with cationic liposomes, considering the expected change in free energy upon polycation−polyanion complex formation. Under the low salt conditions applicable to the present study, the release of the monovalent counterions (Na^+ from DNA, and Cl^- from DOTAP) produces a large entropy gain, which is expected to give a dominant contribution to the change in free energy during the process. As an example, consider the case of CR = 1 for the mixing one mole NCPs having a charge of $-150e$ per NCP "molecule" (due to $-300e$ from the DNA neutralized by $+150e$ from the histone octamer) plus 150 condensed Na^+ ($+150e$) per NCP molecule, with 150 mols DOTAP (in the form of liposomes, each for simplicity assumed to have charge $+150e$) plus 150 condensed Cl^- (charge $-150e$). It can be assumed that ideally, 50% of the NCPs must undergo complete dissociation into histone octamers and DNA for the released DNA to form a charge stoichiometric lamellar structure with DOTAP. This will then result in the release of all condensed monovalent cations and anions to the solution, resulting in maximal entropy gain caused by release of mobile ions. Per mole of initial NCP complex, the released HO, comprising 50% of all initial histones (an average contribution of a charge $+75e$ per initial NCP molecule) will be available for association with the remaining NCPs (charge $-75e$ per initial NCP molecule) forming an electroneutral and most probably disordered phase.

This process predicts the formation of lamellar lipid−DNA as well as DNA−histone domains and the data from confocal and cryo-TEM techniques confirm this prediction. Figure S6 illustrates that the domains enriched with lipid+DNA and DNA +histones do exist. In our previous work[13] using cryo-TEM, domains with no detectable order having sizes on the order of 100 nm were found intermingled among similarly sized domains with an obvious lamellar arrangement in the NCP or array aggregates with 100% DOTAP. However, it should be noted that results from the herein presented confocal microscopy experiments (Figure 3) suggest that the domains of expelled protein can also be significantly larger than those found in the cryo-TEM investigations. This outcome is favored by the almost perfect surface charge matching of DNA rods sandwiched between the cationic lipids. Another factor that can be expected to promote dissociation of the NCPs and the nucleosome arrays is the possibility to alleviate the high bending strain imposed on DNA when it is wrapped around the histone octamer. The estimation of the DNA bending energy in the NCP varies in the range +60 to +150 kJ/mol.[65−67]

Organization of Aggregates at the Intermediate Charge Densities. It should be pointed out that it is likely that some fraction of dissociated histones penetrates the lamellar structure at all bilayer charge densities, favored by mixing entropy and histone−lipid interactions (mostly of hydrophobic nature). This histone inclusion in the lamellar structure is expected to increase when the fraction of DOTAP

is lowered (compared to 100% DOTAP). The presence of an excess of neutral DOPC lipids in the lamellar phase will therefore promote the inclusion of expelled histones into the lipid/DNA lamellar phase. Such a presence of histones would explain the increase in the lamellar distance observed at intermediate charge density of lipid bilayer below 50% DOTAP content (Figure 6 and Figure S3−4). For the precipitates formed with NCPs or arrays, it was noted above that a partial demixing of lipids, caused by a concentration of DOTAP in the vicinity of DNA, is apparently more advantageous than protein inclusion or entrapment of simple counterions in the lamellar structure, down to DOTAP fractions of at least 50%. However, when the DOTAP fraction becomes lower than this, it appears that the retention of a fraction of the cationic histones contributing to the neutralization of DNA becomes advantageous. Histones may also be kinetically trapped between bilayers upon formation of lamellar phase in the non-equilibrium state, as mentioned above.

In the intermediate charge density of bilayers, a decrease in the number of lamellar layers in aggregates with NCPs, arrays, as well as with the corresponding DNA was observed (Figure 7). Such a decrease seems to be augmented by the presence of histones and leads to the liposome−liposome attachments observed in cryo-TEM at 10% DOTAP in aggregates with NCP and arrays, in contrast to multilamellar structures in aggregates with DNA.[13] The decreased interaction potential between DNA and lipid bilayer, due to the neutralization of DNA by histones together with the decreased bilayer charge density, which favors the stability of liposomes thus preventing the formation of lamellar phase, should explain the loss of intensity of lamellar peaks in SAXS spectra.

Organization of Aggregates at the Low Charge Densities. The samples with NCPs and arrays at low fractions of DOTAP constitute a separate group of aggregates that is different from both the aggregates at intermediate and high charge densities, as well as from the samples with DNA molecules in the absence of proteins. The different feature of these samples is the presence of the "NCP peak", which sometimes also coexists with lamellar peaks. These samples also show little or no birefringence under polarized light. The peak broadening indicates that at such low charge densities, only single-layer lamellar domains are formed, which implies that for these aggregates liposomes remain intact. The presence of intact liposomes can explain the density difference of the precipitates between the aggregates with NCPs at low and high lipid charge density. The absence of lamellar peaks and the absence of birefringence indicate that under these conditions, the lamellar phase does not form. Most importantly, the position of the observed peak corresponds well with the distance that would accommodate the lamellar arrangement of a lipid bilayer with intact NCPs in-between.

With lipid bilayers of low charge densities, i.e., bilayers composed of lipid mixtures containing a low fraction of DOTAP, one can expect a relatively large entropic cost in concentrating the charged lipids in certain regions to accommodate a reasonable charge matching on association with an NCP or an array. Consequently, a smaller free energy change is expected to be involved in the association of the components, which will make dissociation of the NCPs or nucleosome arrays as well as formation of multilamellar particles from the closed bilayers of the liposomes less likely. Indeed, previous cryo-TEM investigations show that in samples prepared from NCPs or nucleosome arrays with liposomes containing low fractions of DOTAP, a large fraction of clustered, intact liposomes were present.[13] In the same work, it was also found that, in contrast to cases with corresponding samples containing high fractions of cationic lipid (cf. discussion above), no distinct lamellar domains were observed. The latter observation was taken to suggest that the NCPs/arrays were, at least in part, intact in these samples.

In conclusion, on the basis of the foregoing arguments and observations, one can propose a structure of the precipitate formed with NCPs or nucleosome arrays and liposomes of low cationic charge density, where, as schematically illustrated in Figure 9, intact liposomes are connected by intact NCPs or arrays in a practically random network that may also contain lamellar bilayers with DNA sandwiched in between. This proposed structure is compatible with the observed properties of the precipitates in that (i) The presence of intact liposomes is consistent with a high retention of water; (ii) the structure is overall isotropic, which is consistent with the lack of birefringence in the polarized light microscopy experiments; and, finally, (iii) the observed low-q peak corresponds to characteristic distances in the range of 170−200 Å (see Table 1), which corresponds rather well to the expected distance between two bilayers sandwiching an NCP or an array. Furthermore, the homogeneous appearance of the low-charge density aggregates in the confocal microscopy images discussed above (Figure 3) shows that, in contrast to the case with aggregates prepared with a high fraction of DOTAP, no major sequestering of protein is found in these samples.

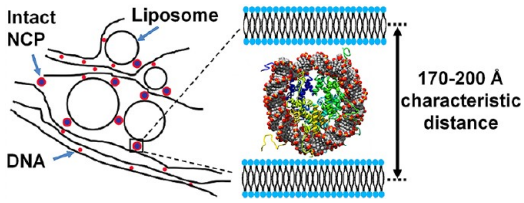

Figure 9. Schematic illustrations of a possible structure of the highly swollen gel formed in samples with liposomes of low charge density (left) and the suggested "unit cell" (right).

CONCLUDING REMARKS

We have here investigated the structures of aggregates formed by either of two different types of "model chromatin" (NCPs or nucleosome arrays) and cationic liposomes of varying charge density. The findings suggest that, with liposomes containing large fractions of cationic lipid, the dominating driving force for aggregation is the increase in translational entropy from the release of the simple counterions of the DNA and the cationic lipid. The ensuing strong DNA−lipid attraction results in the formation of lamellar aggregates of DNA and lipid that are practically identical to those formed with the lipids and DNA alone (i.e., in the absence of proteins), and separate domains of, likely unspecifically aggregated, protein and DNA. With a decreasing fraction of the cationic lipid in the liposomes, an expected tendency for random distribution of the cationic and zwitterionic lipids in the bilayers results in a decreased charge density of the lipid film. This, in turn, makes charge matching between the DNA and the lipids more difficult and concomitantly decreases the gain in entropy from counterion release, which makes a certain extent of inclusion of the net-cationic protein in the lamellar structure more favorable. With

the very lowest fractions of cationic lipid, the DNA−lipid bilayer attraction is weak enough to allow retention of intact NCPs sandwiched between lipid bilayers.

Due to similarities in behavior between mixtures of DNA and cationic lipids and the biologically more directly relevant systems of DNA and zwitterionic or anionic lipids in the presence of divalent ions, the herein presented results can serve as a valuable basis for an improved understanding of the interplay between lipids and chromatin.

■ ASSOCIATED CONTENT

Supporting Information

Figures S1−S6 give additional data that further enhances the main text. This information is available free of charge via the Internet at http://pubs.acs.org/.

■ AUTHOR INFORMATION

Corresponding Author

*E-mail: LarsNor@ntu.edu.sg.

Present Addresses

[‖]CR Competence AB, c/o Center for Chemistry and Chemical Engineering, Lund University, P.O.B. 124, 221 00 Lund, Sweden.

[⊥]Department of Cell Biology, Harvard Medical School, Boston, MA 02115, USA.

Notes

The authors declare no competing financial interest.

■ ACKNOWLEDGMENTS

This work was financially supported by the Biomedical Research Council (A*STAR, Singapore) and by Fundação para a Ciência e a Tecnologia (SFRH/BPD/48522/2008, D.L.). N.V.B. acknowledges the SINGA scholarship from NTU and A*STAR. The National Synchrotron Radiation Research Center (NSRRC) at Hsinchu, Taiwan, and the EMBL (Hamburg, Germany, SAXS beamline) are acknowledged for allocation of beamtime. We acknowledge discussions with Bruno F. B. Silva regarding calculation of the number of layers per domain. We appreciate the linguistic review by Prof. Salil Bose.

■ REFERENCES

(1) Kornberg, R. D. *Annu. Rev. Biochem.* **1977**, *46*, 931−954.
(2) Horn, P. J.; Peterson, C. L. *Science* **2002**, *297*, 1824−1827.
(3) Luger, K.; Mader, A. W.; Richmond, R. K.; Sargent, D. F.; Richmond, T. J. *Nature* **1997**, *389*, 251−260.
(4) Davey, C. A.; Sargent, D. F.; Luger, K.; Maeder, A. W.; Richmond, T. J. *J. Mol. Biol.* **2002**, *319*, 1097−1113.
(5) Routh, A.; Sandin, S.; Rhodes, D. *Proc. Natl. Acad. Sci. U.S.A.* **2008**, *105*, 8872−8877.
(6) Tremethick, D. J. *Cell* **2007**, *128*, 651−654.
(7) Maeshima, K.; Eltsov, M. *J. Biochem.* **2008**, *143*, 145−153.
(8) Ehrenhofer-Murray, A. E. *Eur. J. Biochem.* **2004**, *271*, 2335−2349.
(9) Inagaki, S.; Nakamura, K.; Morikami, A. *PLoS Genet.* **2009**, *5*, e1000613.
(10) Zaina, S.; Dössing, K. B. V.; Lindholm, M. W.; Lund, G. *Curr. Opin. Lipidol.* **2005**, *16*, 549−553.
(11) Ledeen, R. W.; Wu, G. *J. Lipid Res.* **2004**, *45*, 1−8.
(12) Hunt, A. N.; Clark, G. T.; Attard, G. S.; Postle, A. D. *J. Biol. Chem.* **2001**, *276*, 8492−8499.
(13) Lundberg, D.; Berezhnoy, N. V.; Lu, C.; Korolev, N.; Su, C.-J.; Alfredsson, V.; Miguel, M. d. G.; Lindman, B.; Nordenskiöld, L. *Langmuir* **2010**, *26*, 12488−12492.
(14) Radler, J. O.; Koltover, I.; Salditt, T.; Safinya, C. R. *Science* **1997**, *275*, 810−814.
(15) McManus, J. J.; Rädler, J. O.; Dawson, K. A. *Langmuir* **2003**, *19*, 9630−9637.
(16) Liang, H.; Harries, D.; Wong, G. C. L. *Proc. Natl. Acad. Sci. U.S.A.* **2005**, *102*, 11173−11178.
(17) Hughes, G. A. *Nanomedicine* **2005**, *1*, 22−30.
(18) Ewert, K. K.; Evans, H. M.; Zidovska, A.; Bouxsein, N. F.; Ahmad, A.; Safinya, C. R. *J. Am. Chem. Soc.* **2006**, *128*, 3998−4006.
(19) Safinya, C. R.; Ewert, K.; Ahmad, A.; Evans, H. M.; Raviv, U.; Needleman, D. J.; Lin, A. J.; Slack, N. L.; George, C.; Samuel, C. E. *Philos. Trans. R. Soc. A* **2006**, *364*, 2573−2596.
(20) Farago, O.; Ewert, K.; Ahmad, A.; Evans, H. M.; Grønbech-Jensen, N.; Safinya, C. R. *Biophys. J.* **2008**, *95*, 836−846.
(21) Hsu, W.-L.; Li, Y.-C.; Chen, H.-L.; Liou, W.; Jeng, U. S.; Lin, H.-K.; Liu, W.-L.; Hsu, C.-S. *Langmuir* **2006**, *22*, 7521−7527.
(22) Dias, R.; Mel'nikov, S.; Lindman, B. r.; Miguel, M. G. *Langmuir* **2000**, *16*, 9577−9583.
(23) McLoughlin, D. M.; O'Brien, J.; McManus, J. J.; Gorelov, A. V.; Dawson, K. A. *Bioseparation* **2000**, *9*, 307−313.
(24) Wagstaff, K. M.; Fan, J. Y.; De Jesus, M. A.; Tremethick, D. J.; Jans, D. A. *FASEB J.* **2008**, *22*, 2232−2242.
(25) Kott, M.; Haberland, A.; Zaitsev, S.; Buchberger, B.; Morano, I.; Böttger, M. *Somat. Cell Mol. Genet.* **1998**, *24*, 257−261.
(26) Hagstrom, J. E.; Sebestyen, M. G.; Budker, V.; Ludtke, J. J.; Fritz, J. D.; Wolff, J. A. *Biochim. Biophys. Acta, Biomembranes* **1996**, *1284*, 47−55.
(27) Allahverdi, A.; Yang, R.; Korolev, N.; Fan, Y.; Davey, C. A.; Liu, C.-F.; Nordenskiöld, L. *Nucleic Acids Res.* **2011**, *35*, 1680−1691.
(28) Luger, K.; Rechsteiner, T. J.; Richmond, T. J.; Paul, M. W.; Alan, P. W. *Methods Enzymol.* **1999**, *304*, 3−19.
(29) Dyer, P. N.; Edayathumangalam, R. S.; White, C. L.; Bao, Y.; Chakravarthy, S.; Muthurajan, U. M.; Luger, K.; Allis, C. D.; Carl, W. *Methods Enzymol.* **2003**, *375*, 23−44.
(30) Lowary, P. T.; Widom, J. *J. Mol. Biol.* **1998**, *276*, 19−42.
(31) Bimboim, H. C.; Doly, J. *Nucleic Acids Res.* **1979**, *7*, 1513−1523.
(32) Luger, K.; Rechsteiner, T. J.; Richmond, T. J. *Chromatin Protoc.* **1999**, 1−16.
(33) Dorigo, B.; Schalch, T.; Bystricky, K.; Richmond, T. J. *J. Mol. Biol.* **2003**, *327*, 85−96.
(34) Jeng, U. S.; Su, C. H.; Su, C.-J.; Liao, K.-F.; Chuang, W.-T.; Lai, Y.-H.; Chang, J.-W.; Chen, Y.-J.; Huang, Y.-S.; Lee, M.-T.; Yu, K.-L.; Lin, J.-M.; Liu, D.-G.; Chang, C.-F.; Liu, C.-Y.; Chang, C.-H.; Liang, K. S. *J. Appl. Crystallogr.* **2010**, *43*, 110−121.
(35) Bouxsein, N. F.; Leal, C.; McAllister, C. S.; Ewert, K. K.; Li, Y.; Samuel, C. E.; Safinya, C. R. *J. Am. Chem. Soc.* **2011**, *133*, 7585−7595.
(36) Heintzmann, R.; Ficz, G. *Briefings Funct. Genomics Proteomics* **2006**, *5*, 289−301.
(37) Rosevear, F. B. *J. Soc. Cosmet. Chem.* **1968**, *19*, 581−594.
(38) Lasic, D. D.; Strey, H.; Stuart, M. C. A.; Podgornik, R.; Frederik, P. M. *J. Am. Chem. Soc.* **1997**, *119*, 832−833.
(39) Caracciolo, G.; Pozzi, D.; Capriotti, A. L.; Marianecci, C.; Carafa, M.; Marchini, C.; Montani, M.; Amici, A.; Amenitsch, H.; Digman, M. A.; Gratton, E.; Sanchez, S. S.; Laganà, A. *J. Med. Chem.* **2011**, *54*, 4160−4171.
(40) Koltover, I.; Salditt, T.; Safinya, C. R. *Biophys. J.* **1999**, *77*, 915−924.
(41) Piculell, L.; Lindman, B. *Adv. Colloid Interface Sci.* **1992**, *41*, 149−178.
(42) Felgner, P. L.; Gadek, T. R.; Holm, M.; Roman, R.; Chan, H. W.; Wenz, M.; Northrop, J. P.; Ringold, G. M.; Danielsen, M. *Proc. Natl. Acad. Sci. U.S.A.* **1987**, *84*, 7413−7417.
(43) Chesnoy, S.; Huang, L. *Annu. Rev. Biophys. Biomol. Struct.* **2000**, *29*, 27−47.
(44) Anderson, C. F.; Record, M. T. *Annu. Rev. Phys. Chem.* **1995**, *46*, 657−700.
(45) Mascotti, D. P.; Lohman, T. M. *Biochemistry* **1993**, *32*, 10568−10579.

(46) Mascotti, D. P.; Lohman, T. M. *Biochemistry* **1997**, *36*, 7272−7279.
(47) Privalov, P. L.; Dragan, A. I.; Crane-Robinson, C. *Nucleic Acids Res.* **2011**, *39*, 2483−2491.
(48) Korolev, N.; Berezhnoy, N. V.; Eom, K. D.; Tam, J. P.; Nordenskiöld, L. *Nucleic Acids Res.* **2009**, *37*, 7137−7150.
(49) Korolev, N.; Allahverdi, A.; Lyubartsev, A. P.; Nordenskiöld, L. *Soft Matter* **2012**, *8*, 9322−9333.
(50) Korolev, N.; Zhao, Y.; Allahverdi, A.; Eom, K. D.; Tam, J. P.; Nordenskiöld, L. *Biochem. Biophys. Res. Commun.* **2012**, *418*, 205−210.
(51) Eickbush, T. H.; Moudrianakis, E. N. *Biochemistry* **1978**, *17*, 4955−4964.
(52) Ruiz-Carrillo, A.; Jorcano, J. L. *Biochemistry* **1979**, *18*, 760−768.
(53) Evans, D. E.; Wennerström, H. *The Colloidal Domain: Where Physics, Chemistry, Biology and Technology Meet*, 2nd ed.; Wiley-VCH: New York, 1999; Vol. 45.
(54) Dias, R. S.; Miguel, M. G.; Lindman, B. In *DNA Interactions with Polymers and Surfactants*; Dias, R. S., Lindman, B., Eds.; John Wiley & Sons, Inc.: Hoboken, NJ, 2008; pp 367−376.
(55) Machado, A. H. E.; Lundberg, D.; Ribeiro, A. J.; Veiga, F. J.; Miguel, M. G.; Lindman, B.; Olsson, U. *Langmuir* **2010**, *26*, 13102−13109.
(56) Holmberg, K.; Jönsson, B.; Kronberg, B.; Lindman, B. *Surfactants and Polymers in Aqueous Solution*, 2nd ed.; John Wiley & Sons, Ltd: Chichester, U.K., 2003.
(57) Bandyopadhyay, S.; Tarek, M.; Klein, M. L. *J. Phys. Chem. B* **1999**, *103*, 10075−10080.
(58) Leal, C.; Sandström, D.; Nevsten, P.; Topgaard, D. *Biochim. Biophys. Acta, Biomembranes* **2008**, *1778*, 214−228.
(59) Dias, R. S.; Pais, A. A. C. C.; Linse, P.; Miguel, M. G.; Lindman, B. *J. Phys. Chem. B* **2005**, *109*, 11781−11788.
(60) Khalid, S.; Bond, P. J.; Holyoake, J.; Hawtin, R. W.; Sansom, M. S. P. *J. R. Soc. Interface* **2008**, *5*, 241−250.
(61) Farago, O.; Grønbech-Jensen, N. *Biophys. J.* **2007**, *92*, 3228−3240.
(62) McManus, J. J.; Radler, J. O.; Dawson, K. A. *J. Am. Chem. Soc.* **2004**, *126*, 15966−15967.
(63) Salditt, T.; Koltover, I.; Rädler, J. O.; Safinya, C. R. *Phys. Rev. Lett.* **1997**, *79*, 2582.
(64) Wong, G. C. L.; Tang, J. X.; Lin, A.; Li, Y.; Janmey, P. A.; Safinya, C. R. *Science* **2000**, *288*, 2035−2039.
(65) Widom, J. *Q. Rev. Biophys.* **2001**, *34*, 269−324.
(66) Schiessel, H. *J. Phys.: Condens. Matter* **2003**, *15*, R699.
(67) Flaus, A.; Owen-Hughes, T. *Biopolymers* **2003**, *68*, 563−578.